Ultrathin MOF nanosheet assembled highly oriented microporous membrane as an interlayer for lithium-sulfur batteries☆

Meng Tian[a,1], Fei Pei[b,1], Mingshui Yao[a], Zhihua Fu[a], Lele Lin[b], Guodong Wu[a], Gang Xu[a,c,*], Hiroshi Kitagawa[d], Xiaoliang Fang[b,**]

[a] State Key Laboratory of Structural Chemistry, Fujian Institute of Research on the Structure of Matter, Chinese Academy of Sciences, Fuzhou, Fujian 350002, China
[b] Pen-Tung Sah Institute of Micro-Nano Science and Technology, Xiamen University, Xiamen, Fujian 361005, China
[c] University of Chinese Academy of Sciences, Chinese Academy of Sciences, Beijing 100039, China
[d] Division of Chemistry, Graduate School of Science, Kyoto University, Kitashirakawa Oiwake-cho, Sakyo-ku, Kyoto 606-8502, Japan

ARTICLE INFO

ABSTRACT

Lithium sulfur (Li-S) batteries are attracting increasing attentions as promising next-generation rechargeable batteries. However, the rapid capacity fading of sulfur cathodes caused by the shuttling of polysulfide intermediates between the cathodes and anodes restricts the application of Li-S batteries. In this work, a facile wet-chemistry method is developed for the direct synthesis of few-molecular-layer thin metal-organic framework (MOF) nanosheets without using surfactant. By assembling these ultrathin MOF nanosheets with a facile vacuum filtration method, a highly oriented and flexible MOF membrane with favorable mechanical properties is achieved for the first time. The excellent features make the as-prepared MOF nanosheets ideal to fabricate lightweight interlayer modified separators for suppressing the polysulfide shuttling of Li-S batteries. When using the MOF membrane modified separator, the Li-S batteries made from commercial carbon materials exhibits the significantly enhanced cycling stabilities. This work brings new opportunities for the synthesis and application of MOF materials.

1. Introduction

The booming development of portable electronics and electric vehicles has inspired growing demand on developing the next generation rechargeable batteries. Among existing candidates, lithium-sulfur (Li-S) batteries have been under spotlight in the past decade due to their theoretical specific energy of 2600 Wh kg^{-1} and the cost effectiveness, abundance, and nontoxicity of sulfur [1–4]. However, the insulating nature of sulfur, the dissolution of polysulfide intermediates (Li$_2$S$_n$, $4 \leq n \leq 8$) in electrolytes with a "shuttle effect", and the large volume change of sulfur during lithiation/delithiation process lead to low sulfur utilization and fast capacity fading of sulfur cathodes, thus limiting the practical application of Li-S batteries [1–5]. To address these issues, tremendous efforts have been devoted to improving the capacities and cycling stabilities of sulfur cathodes by designing the sulfur-hosting materials [6–17]. During in the past few years, placing an

interlayer between the cathode and the separator that can block polysulfide but transport Li$^+$ has emerged as a convenient to suppress the migration of polysulfides from the cathode side to the anode side [18–21]. This strategy not only can effectively alleviate the "shuttle effect", but also has the potential to reduce the cost of sulfur cathode by only using commercial carbon materials as the sulfur-hosting materials. It's worth noting that the use of interlayer will also decrease the sulfur content in the battery. Unfortunately, many of the barrier layers reported previously are of high weight density [22–24]. Therefore, designing lightweight and high-performance interlayers for Li-S batteries is highly desired.

Metal-organic frameworks (MOFs) are one class of crystalline, porous materials with designable structure and tunable properties. They have burgeoning applications particularly in separation, gas storage, catalysis, sensing, and energy conversion and storage [25–30]. With favorable porous structures and polysulfide-binding abilities, MOF
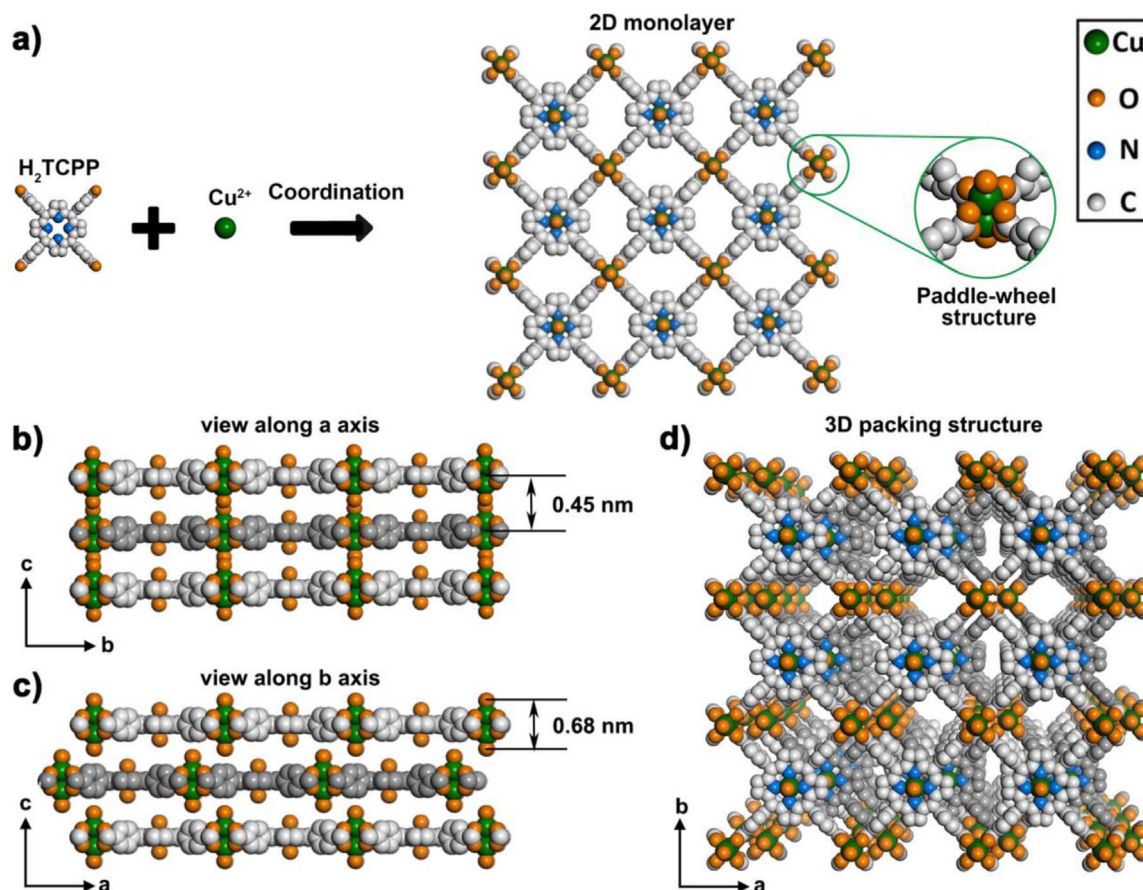
Fig. 1. Simulated crystal structure of Cu$_2$(CuTCPP).

materials have been investigated as the sulfur-hosting materials to construct MOF/S composite cathodes and suppress the polysulfide shuttling of Li-S batteries [28–30]. Since most of MOFs are non-conductive and cannot directly help increasing the conductivity of sulfur cathodes, the MOF/S composite cathodes usually requires some additional procedures (e.g., adding or coating with conductive materials) to improve the sulfur utilization [31]. The homemade separator composed of the MOF particles and graphene oxide nanosheets reported recently indicate that using the molecular sieving ability of MOF materials is a good choice for the application of MOF materials in Li-S batteries [32]. Theoretically, MOF films/membranes with the uniform microporous structure are the ideal candidates for the interlayers. However, the high-quality thin MOF films/membranes with good crystallinities, highly oriented porous structures, and controlled thicknesses are extremely attractive but challenging to be prepared [33–35]. At present, such a high-quality MOF thin film/membrane can be successfully fabricated with the well-developed layer-by-layer liquid epitaxy method [36–38]. In layer-by-layer liquid epitaxy method, the organic self-assembled mono-layer (SAM) on the surface of the substrate plays a key role in leading the oriented growth of MOF thin film. Thus, a smooth solid substrate for growing organic SAM is critical to this method, while limiting this method to be used to prepare a MOF membrane. Because a membrane is a thin film with permeable structure and therefore is required to possess a self-supporting structure or grow on a porous substrate. How to develop a facile, fast, and low-cost route to prepare high-quality MOF membrane with controllable structural parameters still remains a big challenge.

Ultrathin two-dimensional (2D) crystals, such as graphene, transition metal chalcogenides and transition metal oxides are useful building blocks for assembling large-area membranes [39–42]. Many methods, like filtration, self-assembly, centrifugal evaporation and tap casting have been developed for this purpose [43–45]. Inspired by these convenient methods, we report herein a straightforward method for the synthesis of few-molecular-layer thin copper-based MOF nanosheets. As expected, a highly oriented MOF membrane is able to be efficiently prepared by vacuum filtering the ultrathin MOF na-nosheets suspension. Impressively, the as-prepared MOF membrane possesses not only highly-oriented porous structure but also controlled thickness, scalable lateral size. These excellent features enable this MOF membrane to have great potentials in sieving applications. As a result, when used as an interlayer, the lightweight copper-based MOF membrane remarkably enhanced the cyclic performance and rate capability of the carbon/sulfur cathodes made from commercial carbon materials. Ultrathin MOF nanosheet assembled highly oriented micro-porous membrane reported in this work provides new insights into the applications of MOF materials in Li-S batteries.

2. Results and discussion

2.1. Synthesis and characterizations of ultrathin MOF nanosheets

The crystalline MOF nanosheets with few-molecular-layer thick-ness, Cu$_2$(CuTCPP) (TCPP = 5, 10, 15, 20-tetrakis (4-carboxyphenyl) porphyrin), are successfully prepared in high yield by a one-pot solution reaction of Cu(NO$_3$)$_2$·3H$_2$O and H$_2$TCPP in N, N-dimethyl-formamide (DMF) at 85 °C for 24 h (for details, see the experimental section). Although Cu$_2$(CuTCPP) possesses a 2D crystal structure and has a trend to spontaneously grow anisotropically into a sheet-like morphology, the synthesis of few-molecular-layer thin Cu$_2$(CuTCPP) nanosheets without surfactant has not yet been achieved [38]. We found that the use of DMF as the solvent and controlling the concentration of the reagents are the key factors for manipulating the

thickness of the nanosheets. Higher concentrations of the reagents resulted in nanosheets with thicknesses of hundreds of nanometers (Fig. S1). In contrast, at lower concentrations, high-aspect-ratio nanosheets with good dispersion could be obtained. The nanosheets with diameters of several micrometers and thickness of ~3.0 nm were obtained using ligand and metal salt concentrations lower than 6.0×10^{-4} and 2.0×10^{-3} mol L^{-1}, respectively.

As shown in Fig. 1, the $Cu_2(CuTCPP)$ nanosheets have a porous 2D reticulated structure constructed by porphyrin ligands and Cu^{2+} ions [40]. The carboxyl groups of every four neighboring porphyrin ligands bond to two Cu^{2+} ions to form a binuclear $Cu_2(COO)_4$ paddle-wheel structure through coordination interaction (Fig. 1). The Cu-centered porphyrin ligands are connected through these paddle-wheel structures resulting in a 2D reticulate layer in the *ab*-plane of the structure. Along the c-axis, the reticulate layers are assembled through van der Waals interactions in an AB mode where the B layer is shifted from the vertical position of the A layer by ¼ of the unit cell along the *a*-axis (Fig. 1). The AB packing of the reticulate layers produces 1D channels along the c-axis with an open window size of ~1.0 nm (Fig. 1). These uniform microporous channels are smaller than the diameters of the long-chain polysulfide intermediates of Li-S batteries and can be used as a sieve for blocking polysulfides [32]. The powder X-ray diffraction (XRD), Fourier-transform infrared spectrum, and gas sorption measurements confirm this crystal structure very well (Fig. 2a–c). Compared with the spectrum of H_2TCPP, $Cu_2(CuTCPP)$ shows highly reduced intensities of peaks at around 1700 cm^{-1} and 1260 cm^{-1}, which confirms the formation of $Cu_2(COO)_4$. The disappearance of the peak at ~966 cm^{-1} is due to the coordination of Cu and N in the pyrrole ring. The transmission electron microscope (TEM) image reveals that the $Cu_2(CuTCPP)$ nanosheets have a smooth surface, with uniform and ultrathin thickness (Fig. 2d and S2). The different contrast in the TEM image is due to the fold on the nanosheet, demonstrating the flexibility of this high aspect ratio material (Fig. S2). Sharp and ordered spot arrays in the selected-area electron diffraction (SAED) patterns in Fig. 2e clearly indicate that the nanosheet is single crystalline and has a tetragonal ordered structure parallel to the TEM grid. From this

diffraction data, the lattice constants are calculated to be $a = b = 16.50$ Å and agree well with the crystal structure in the *ab* plane. Atomic force microscope (AFM) measurements show the nanosheets have the homogeneous thickness of ~3.0 nm, indicating that there are only ~7 reticular layers in one nanosheet (Fig. 2f and S3). Notably, the direct synthesis of few-molecular-layer MOF nanosheets in a large scale has been seldom reported [46].

2.2. Ultrathin MOF nanosheets assembled membrane

The prepared $Cu_2(CuTCPP)$ nanosheets have good dispersion in ethanol (the inset of Fig. 2c). Therefore, a large area and well-ordered MOF membrane can be conveniently obtained by the vacuum filtration of this nanosheet suspension (Fig. 3a and S4) [47,48]. Grazing-incidence XRD and out-of-plane XRD were employed to investigate the assembly structure of $Cu_2(CuTCPP)$ nanosheets, as they are sensitive to the lattice information parallel (in-plane) and perpendicular (out-of-plane) to the membranes, respectively. The sharp peaks in the XRD patterns (Fig. 3b and c) indicate the crystalline feature of the membranes; all the in-plane peaks can be assigned to *hk*0, while the out-of-plane peaks can be assigned to 00*l*. These results suggest that the nanosheets in the membranes are highly oriented with stacking along the *c* axis of the crystal structure. The cross-section scanning electron microscope (SEM) image of the membrane also confirms that the nanosheets in the membrane stack parallel to one-another and form a densely packed "brick wall", resulting in a highly-oriented structure (Fig. 3d and S5). In addition, the thickness of the membranes linearly depends on the quantity of $Cu_2(CuTCPP)$ nanosheets and can be easily controlled from tens of micrometers to hundreds of micrometers (Fig. 3e). The area of the membrane can also be easily scaled up by using larger filter (the inset in Fig. 3d).

MOF crystal is very fragile in general. Surprisingly, the prepared $Cu_2(CuTCPP)$ membranes have excellent mechanical flexibility, due to the profound van der Waals interaction between the large transverse dimensions of ultrathin MOF nanosheets. Fig. 3f and S6 show that a ~50-μm-thick membrane could be repeatedly bent and relaxed for at
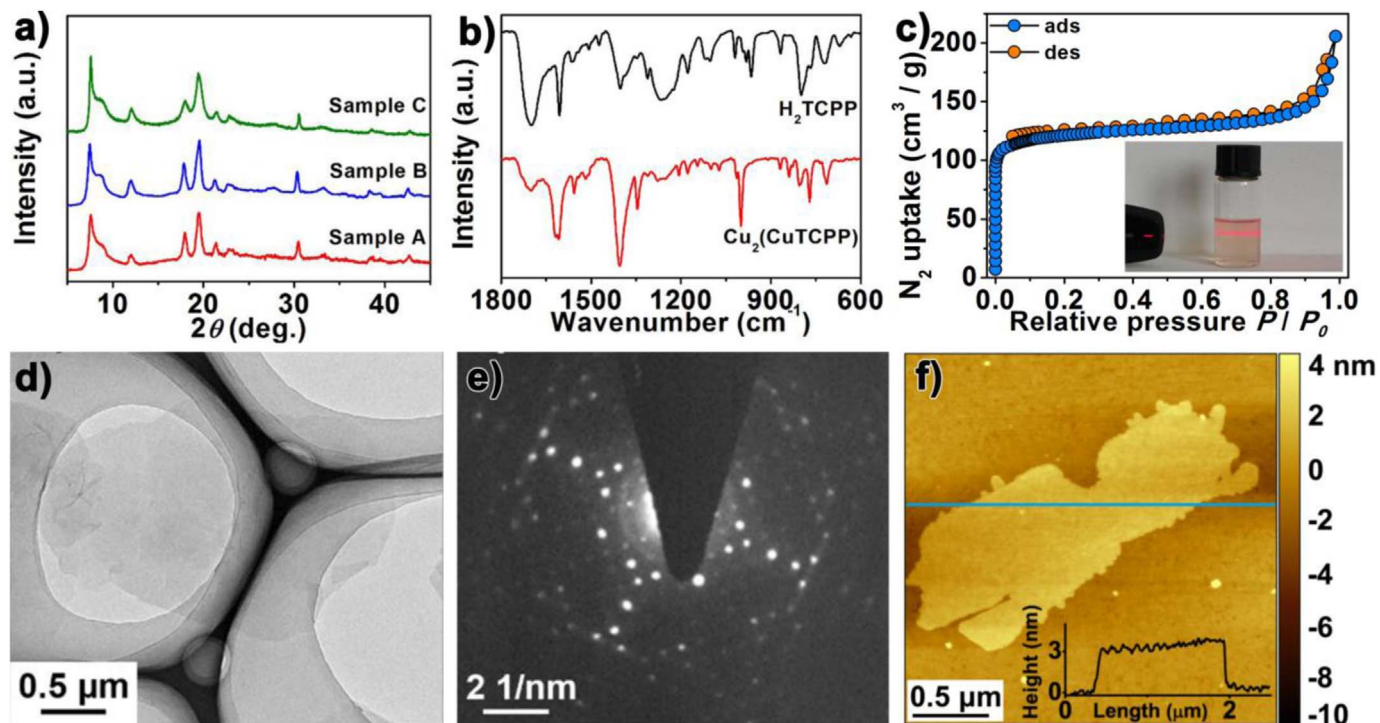
Fig. 2. Powder XRD of the samples prepared using different concentrations of reagents (a). FT-IR spectra of H_2TCPP and $Cu_2(CuTCPP)$ nanosheets (b). N_2 sorption isotherms of $Cu_2(CuTCPP)$ membrane at 77 K (c, the inset is the Tyndall effect of the colloidal suspension of $Cu_2(CuTCPP)$ nanosheets). Characterizations of the $Cu_2(CuTCPP)$ nanosheets: TEM image (d), SAED pattern (e), and AFM image (f, the inset: the height profile of the nanosheet along the blue line).
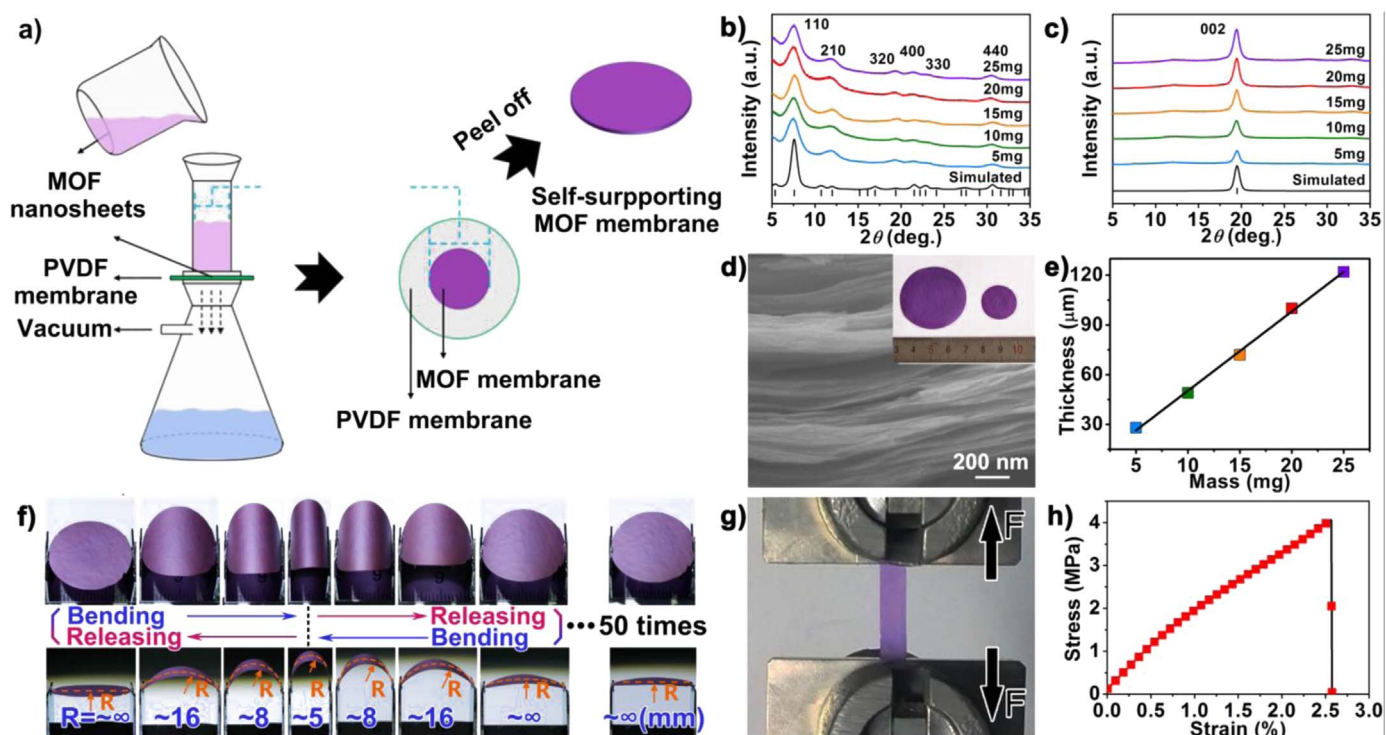
Fig. 3. Schematic image for the preparation of Cu$_2$(CuTCPP) membrane (a). In-plane (b) and out-of-plane (c) XRD patterns of the Cu$_2$(CuTCPP) membrane with different mass (i.e., different thickness). Cross-section SEM image of the Cu$_2$(CuTCPP) membrane (d); inset: the photographs of the membranes with controllable sizes. Mass-dependent thickness plots of the membrane (e). Bending and relaxing processes of the membrane with the thickness of ~50 μm and the diameter of 2.0 cm (f). Stress-strain measurement of the Cu$_2$(CuTCPP) membrane (g). Typical stress-strain curve of a 50-μm-thick membrane (h).

least 50 times without any visible cracks. The minimum radius of curvature of the membrane in this process is 5 mm which is similar to that of graphene oxide membrane (~2.3 mm) [49]. The stress-strain measurement of the 50-μm-thick membrane was also performed along the direction parallel to the membrane surface (Fig. 3g and h). The strain curve of the membrane almost linearly increases during tensile loading. After that, the curve has a sudden decrease due to the rupture of the membrane [50–52]. The ultimate tensile stress for the membrane is 4.1 MPa (average from three tested samples) and comparable to those of the graphene, carbon nanotube, WS$_2$ and MoS$_2$ membranes made by similar filtration method (Tab. S1 and S2) [50–52]. The Young's modulus is calculated to be ~0.17 GPa in average, which is at the same level of BN, bucky paper and MoS$_2$ [50–52].

2.3. Application of MOF membrane in Li-S batteries

Although the ultrathin MOF nanosheets assembled interlayers have not been reported until now, it can be predicted that the Cu$_2$(CuTCPP) nanosheets with highly oriented microporous structures have great potential for improving the performance of Li-S batteries. To alleviate the decrease of the overall energy density aroused from the use of interlayers, an available strategy is to construct a lightweight interlayer on one surface of commercial Celgard separator, as the weight and thickness of Cu$_2$(CuTCPP) membrane can be easily controlled using Celgard separator as both the filter membrane and the substrate [53–56]. In addition, such an interlayer modified separator is also very convenient for battery assembling. Following this strategy, a 500 nm thick Cu$_2$(CuTCPP) membrane (Fig. S7) with mass loading of 0.1 mg cm^{-2} was fully coated on the macroporous surface of commercial Celgard separator through the vacuum filtration method, resulting in a lightweight interlayer modified separator (for details see experimental section).

As demonstrated by the model polysulfide Li$_2$S$_6$ (Fig. 4a), the Cu$_2$(CuTCPP) membrane can significantly reduce the permeability of

polysulfides through Celgard separator. Compared with the Celgard separator, the favorable polysulfide-trapping ability of the Cu$_2$(CuTCPP) membrane is mainly attributed to the uniform microporous feature and densely packed structure of ultrathin Cu$_2$(CuTCPP) nanosheets (Fig. 3d). The oriented assembly of ultrathin Cu$_2$(CuTCPP) nanosheets on the macroporous Celgard separator formed an ideal physical barrier layer and suppressed the migration of polysulfides (Fig. S8) [53–56]. In addition, both the infrared (IR) spectrum and X-ray photoelectron spectroscopy (XPS) of the Cu$_2$(CuTCPP) membrane after Li$_2$S$_6$ permeation measurement reveals that ultrathin Cu$_2$(CuTCPP) nanosheets have a relatively strong interaction with polysulfides, which is beneficial for improving the polysulfide-trapping ability of the Cu$_2$(CuTCPP) membrane (Figs. S9 and S10) [31–33]. As shown in Fig. 4b, Li-S coin cells were assembled by employing the Cu$_2$(CuTCPP) membrane modified Celgard separator or Celgard separator (referred as Cu$_2$(CuTCPP)-Celgard and Celgard) to investigate the application the potential application of ultrathin Cu$_2$(CuTCPP) nanosheets. High sulfur content cathodes (64–70 wt% of sulfur) with area sulfur loading from 2.0 to 10.0 mg cm^{-2} were constructed by using the commercial carbon materials (e.g., carbon black (CB) or carbon nanotubes (CNT)) as the sulfur-hosting materials (Fig. S11). It should be pointed out that the sulfur contents of these C/S cathodes are higher than many other Li-S cathodes reported previously [57]. Although Cu$_2$(CuTCPP) is non-conductive, the oriented pore in the membrane guarantees the shortest way for Li$^+$ transport in the membrane. As results, the electrochemical impedance spectra of the Cu$_2$(CuTCPP)-Celgard and Celgard cells with the CB/S cathodes (64 wt% and 2.0 mg cm^{-2} of sulfur in cathodes) revealed that Cu$_2$(CuTCPP) membrane does not deteriorate the charge transfer of batteries due to its ultrathin and pore-oriented natures (Fig. 4c).

In order to assess the performance of the Cu$_2$(CuTCPP) membrane, two coin cells were firstly activated at 0.05 C (1 C = 1675 mA g^{-1}) for 1 cycle, and then cycled at 0.2 C for 100 cycles (Fig. 4d ~ f). Two reaction plateaus at 2.3 and 2.1 V observed in both the Cu$_2$(CuTCPP)-Celgard
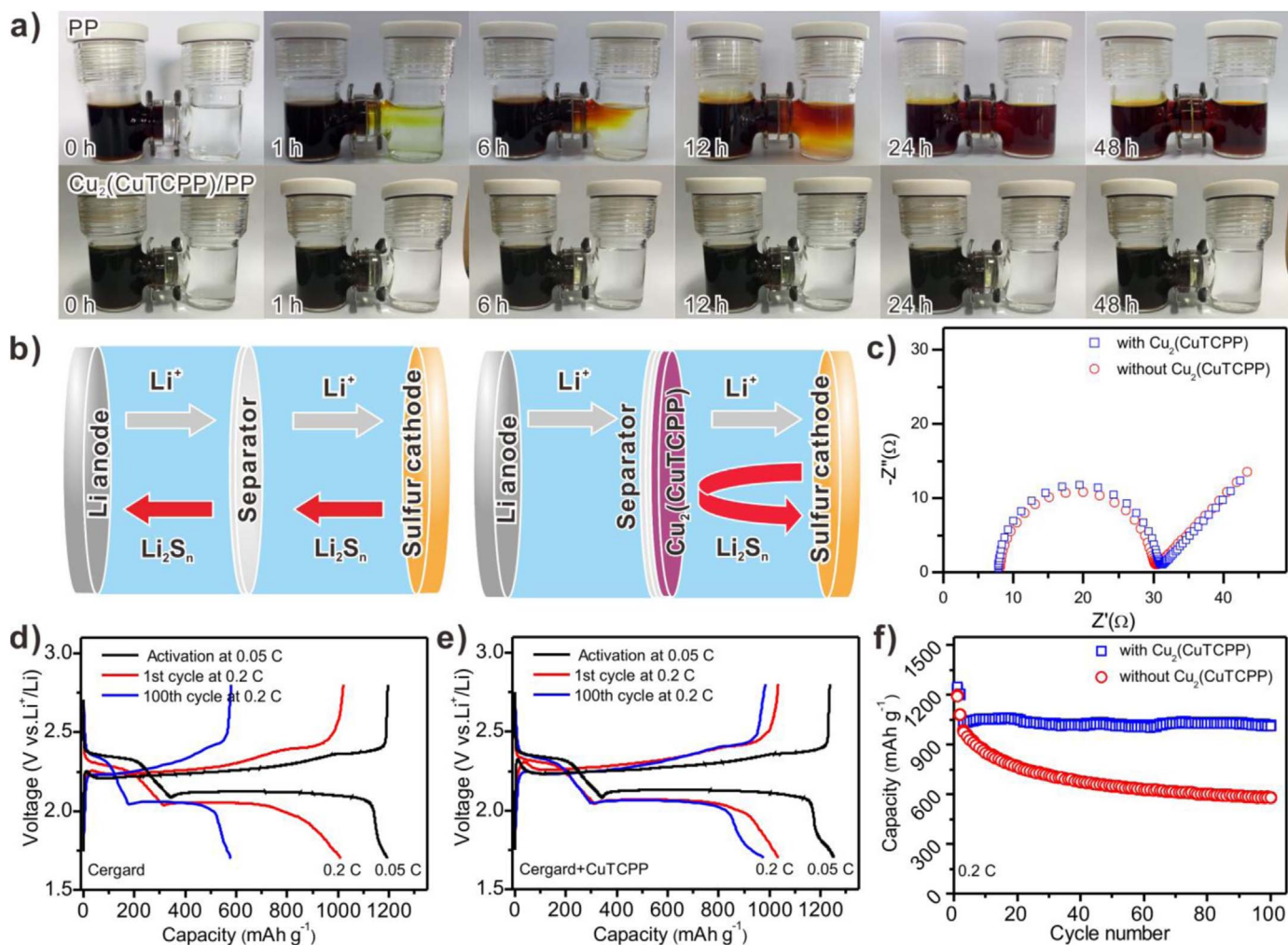
Fig. 4. Polysulfide permeation measurements for the Celgard and Cu$_2$(CuTCPP)-Celgard separators (a). Schematic illustration of the Celgard and Cu$_2$(CuTCPP)-Celgard cells (b). Electrochemical impedance spectra of the freshly prepared Celgard and Cu$_2$(CuTCPP)-Celgard cells with the CB/S cathodes (c). Charge/discharge curves at 0.2 C: the Celgard cell with the CB/S cathode (d) and the Cu$_2$(CuTCPP)-Celgard cell with the CB/S cathode (e). Cycling performance of the Celgard and Cu$_2$(CuTCPP)-Celgard cells with the CB/S cathodes at 0.2 C (f).

and Celgard cells are corresponding to the typical two-stage conversion reaction from S$_8$ → Li$_2$S$_{8-4}$ → Li$_2$S$_2$/Li$_2$S, confirming that of the Cu$_2$(CuTCPP) membrane does not affect the chemical reaction of sulfur cathode [1–3]. As shown in Fig. 4g, the initial discharge capacities at 0.05 C calculated based on the weight of sulfur are around 1200 mAh g^{-1} for the Cu$_2$(CuTCPP)-Celgard and Celgard cells. The similar sulfur utilizations suggest that the Li$^+$ can smoothly run through Cu$_2$(CuTCPP) membrane [53–56]. More importantly, after 100 cycles at 0.2 C, the discharge capacity of the Cu$_2$(CuTCPP)-Celgard cells (1020 mAh g^{-1}) is significantly higher than that of the Celgard cell (580 mAh g^{-1}). It is attributed to the preferable polysulfide-trapping ability of the Cu$_2$(CuTCPP) membrane, which is beneficial to alleviate the migration of polysulfides from the cathode to the anode. Additionally, the SEM and PXRD measurements reveal that the Cu$_2$(CuTCPP) membrane are highly stable during the charge-discharge process (Figs. S12 and S13).

The Cu$_2$(CuTCPP) membrane also can improve the rate capability of Li-S batteries (Fig. 5a–c and S14). When cycled at 0.2, 0.5, 1, 2, 3, 4, and 5 C, the discharge capacities of the Cu$_2$(CuTCPP)-Celgard cell with the CB/S cathode were 953, 849, 781, 636, 570, 510, and 437 mAh g^{-1}, respectively. Notably, even at a high current density rate of 5 C, the obvious discharging platform can still be observed for the Cu$_2$(CuTCPP)-Celgard cell. In contrast, the discharge capacity of the

Celgard cell with the CB/S cathode decayed quickly with the increase of current density rate. The discharge capacity of the Celgard cell at 5 C was only about 60 mAh g^{-1}. To further evaluate the long-term cycling stabilities, the Cu$_2$(CuTCPP)-Celgard and Celgard cells were carried out at a high rate of 1 C (Fig. 5d, e and S15). The Cu$_2$(CuTCPP)-Celgard cell with the CB/S cathode delivers an initial discharge capacity of 850 mAh g^{-1} after 1 cycle of activation at 0.05 C. After 900 cycles at 1 C, the final capacity is 604 mAh g^{-1} with capacity retention of 71.1%, corresponding to an ultralow capacity decay of 0.032% per cycle. In a sharp contrast, the Celgard cell with the CB/S cathode exhibits a fast capacity loss during 200 cycles (from 1173 to 156 mAh g^{-1}), confirming that the Cu$_2$(CuTCPP) membrane is an efficient barrier layer for increasing the lifespan of Li-S batteries (Tab. S4). During the cycling tests, the internal resistance of the Cu$_2$(CuTCPP)-Celgard cell with the CB/S cathode remained stable (Fig. S16). In addition, the corrosion of the Li anode caused by the side reactions between polysulfides and Li has also been significantly reduced in the Cu$_2$(CuTCPP)-Celgard cell, as the polysulfides have been confined within the cathode side (Fig. S17). More importantly, we also demonstrated that the Cu$_2$(CuTCPP) membrane has a good potential in constructing high-sulfur-loading Li-S batteries. When using the Cu$_2$(CuTCPP)-Celgard separators, the CNT cathodes with 70 wt% and 4, 7, and 10 mg cm^{-2} of sulfur can deliver high areal capacities of 4.05, 6.75, and 9.22 mA h cm^{-2}, respectively, after 100 cycles at
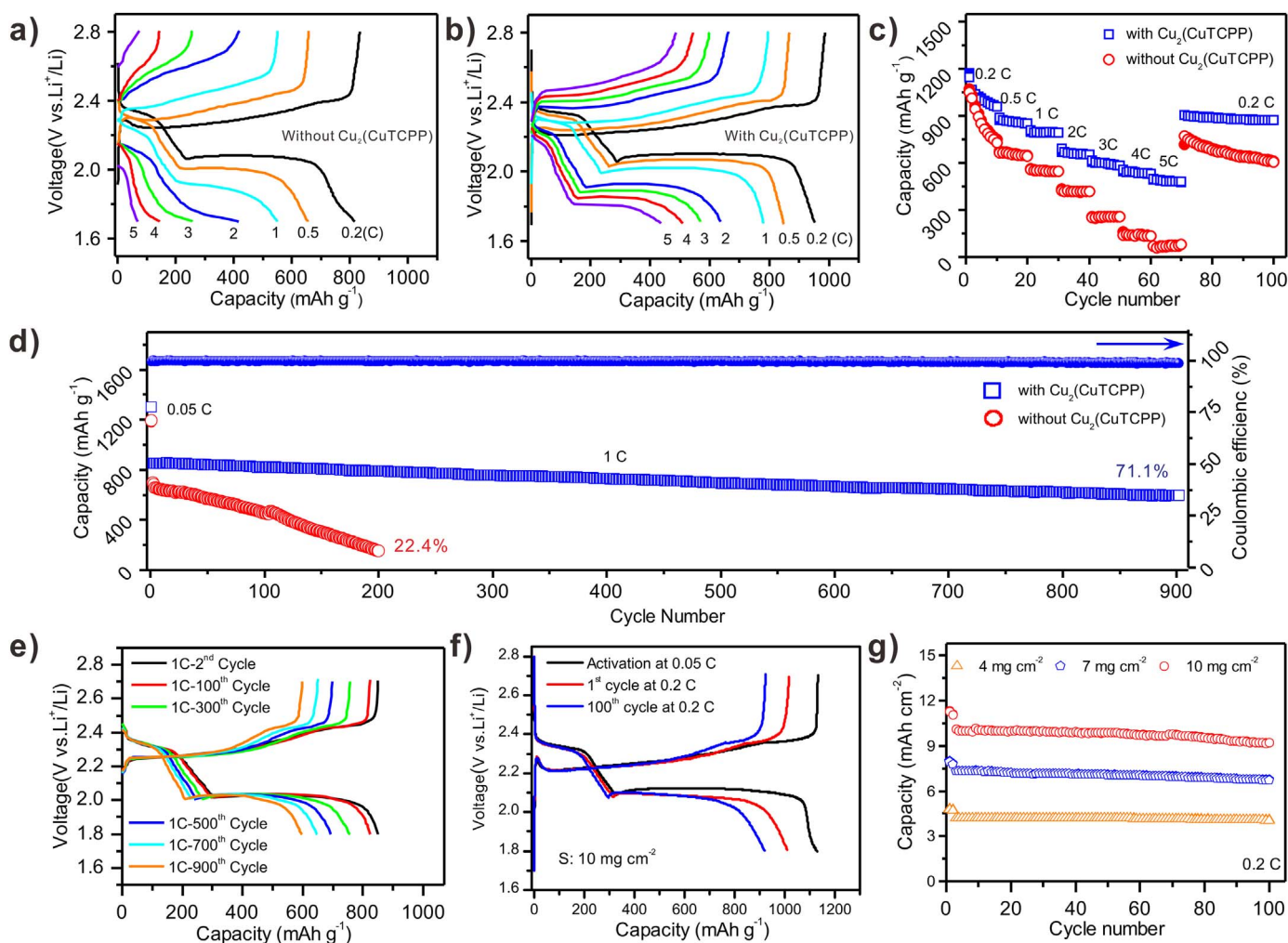
Fig. 5. Charge/discharge curves at different density rates: the Celgard cell with the CB/S cathode (a) and the Cu$_2$(CuTCPP)-Celgard cell with the CB/S cathode (b). Rate capabilities of the Celgard and Cu$_2$(CuTCPP)-Celgard cells with the CB/S cathodes (c). Cycling performance of the Celgard and Cu$_2$(CuTCPP)-Celgard cells with the CB/S cathodes at 1 C (d). Charge/ discharge curves of the Cu$_2$(CuTCPP)-Celgard cell with the CB/S cathode at 1 C (e). Charge/discharge curves of the Cu$_2$(CuTCPP)-Celgard cell with the CNT/S cathode (70 wt% and 10 mg cm^{-2} of sulfur) at 0.2 C (f). Cycling performance of the Cu$_2$(CuTCPP)-Celgard cells with the CNT/S cathodes (70 wt% and 4–10 mg cm^{-2} of sulfur) at 0.2 C (g).

0.2 C (Fig. 5f, g and S18), higher than the state-of-the-art Li-ion batteries (~4 mA h cm^{-2}) [57]. These results not only highlighted the favorable performance of ultrathin Cu$_2$(CuTCPP) nanosheets, but also indicated that designing ultrathin MOF nanosheet and its derived MOF membrane is a promising strategy for the application of MOF martials in high-energy Li-S batteries.

3. Conclusion

In conclusion, a crystalline few-molecular-layer thin Cu$_2$(CuTCPP) nanosheet was directly synthesized in high yield by a one-pot solution method without surfactant. Based on this ultrathin nanosheet, a Cu$_2$(CuTCPP) membrane with high orientation, controlled thickness, large lateral size and good flexibility was achieved by the vacuum-assisted filtration method. We demonstrated the lightweight and highly oriented Cu$_2$(CuTCPP) membrane can be used as a high-performance interlayer to effectively suppress polysulfide shuttling and improve the cycling stabilities of Li-S batteries. By using the Cu$_2$(CuTCPP) modified separator, the slurry-coated CB/S cathode exhibited a high capacity retention of 71.1% after 900 cycles 1 C. The high-sulfur-loading CNT/S cathode with 70 wt.% and 10 mg cm^{-2} of sulfur delivered a high areal capacity of 9.22 mA h cm^{-2} after 100 cycles at 0.2 C. We believe that this work not only provides a promising route to develop high-energy Li-S batteries,

but also could bring inspiration on the preparation of other MOF or covalent organic framework materials into high-quality membranes for other applications, such as catalysis, gas separation, and fuel cells.

4. Experimental section

4.1. Materials

All chemicals were purchased from Tokyo Chemical Industry Co., and Sinopharm Group Co. Ltd. and used without further purification.

4.2. Preparation of Cu$_2$(CuTCPP) nanosheets

Cu$_2$(CuTCPP) nanosheets were synthesized using a solvothermal reaction of Cu(NO$_3$)$_2$·3H$_2$O and H$_2$TCPP (5,10,15,20-tetrakis (4-carboxyphenyl) porphyrin) in *N, N*-diethylformamide (DMF). Typically, H$_2$TCPP (7.9 mg, 0.01 mmol), Cu(NO$_3$)$_2$·3H$_2$O (7.3 mg, 0.03 mmol), DMF 3 mL (for sample A), 6 mL (for sample B), 18 mL (for sample C), were mixed at room temperature. The mixture was heated up to 35 °C during 1 h and kept at that temperature for 10 h; then heated up to 85 °C in 10 h and kept threat for one day. The container was then gradually cooled to room temperature at the rate of 5 °C h^{-1} and a purple sample was obtained. The SEM images of samples A, B, and C are shown in Fig. S1.

4.3. Fabrication of Cu₂(CuTCPP) self-supporting membrane

Cu$_2$(CuTCPP) ultrathin nanosheets were dispersed in ethanol by ultrasonication at the concentration of 0.1 g L^{-1}. Then, the nanosheet suspension with the appropriate volume (50, 100, 150, 200, or 250 mL) was filtered using a vacuum through a PVDF filter membrane (pore size of 450 nm) in the setup of diameter of 2 cm. After drying, the self-supporting MOF membrane with 2 cm diameter was detached. The membranes could be fabricated in various thicknesses. The membrane with 4 cm diameter was fabricated by the same method using a setup of diameter of 4 cm.

4.4. Fabrication of Cu₂(CuTCPP)-Celgard separator

25 mg of Cu$_2$(CuTCPP) was dispersed into 50 mL of ethanol by ultrasonication for 10 min. Then, 18 mL of the Cu$_2$(CuTCPP) dispersion and 1.0 mL of 0.2 wt% N-lauryl acrylate (LA133) aqueous solution were ultrasonication for 5 min. The as-prepared dispersion was vacuum filtered on the Celgard separator, and then washed with ethanol. The obtained Cu$_2$(CuTCPP)-Celgard separator was dried at 60 °C for 6 h and the Cu$_2$(CuTCPP) membrane layer on the Celgard separator was controlled to be 0.1 mg cm^{-2}. It should be pointed out that the polymer binders are usually used in literature to enhance adhesion between the barrier layer and separator, which can also prevent the disintegration of the barrier layers in the electrolyte [56]. The control experiment reveals that LA133 cannot suppress the shuttle effect of Li-S batteries (Fig. S19).

4.5. Fabrication of the C/S cathodes

The C/S cathodes used in this work were fabricated by employing the low-cost commercial carbon black (CB) or carbon nanotubes (CNT) as the sulfur-hosting materials. The CB/S composite with 80 wt% of sulfur was prepared by heating the mixture of CB and sulfur (1:4, w/w) at 155 °C for 12 h in a sealed glass bottle. The CB/S composite cathode was further prepared by the slurry-coating method. The slurry was prepared by mixing CB/S composites, CB and LA133 in a weight ratio of 80:10:10 in ethanol and deionized water. The slurry was then spread on the Al foil and dried in a vacuum oven at 60 °C for 12 h, resulting in the slurry-coated CB/S cathode. The sulfur content and area sulfur loading of the CB/S cathodes are 64% and 2.0 mg cm^{-2}, respectively.

The CNT/S composite was prepared and used as the cathodes with higher areal sulfur loading, Typically, 10 g of commercial CNT was dispersed into 10 mL of Triton X-100 aqueous solution (0.01 wt%) by ultrasonication for 0.5 h. The obtained CNT aqueous dispersion was vacuum filtered through 0.45 mm of nylon film. After washing and drying processes, the free-standing CNT paper was peeled from the filter. The CNT paper was further cut into small plates. The S/CS$_2$ solution was dropped into the CNT plates, and then heated at 155 °C for 6 h in a sealed glass bottle. The resulting CNT/S plates with sulfur content of 70 wt.% were directly used as the cathodes. By controlling the dosages of CNT and S/CS$_2$ solution, the areal sulfur loading of the CNT/S cathodes used in this work are 4, 7, and 10 mg cm^{-2}, respectively.

4.6. Characterizations

Powder X-ray diffraction (PXRD) analysis was performed by a MiniFlex2 ×-ray diffractometer using Cu-K$_\alpha$ radiation (λ = 0.1542 nm) in the 2θ range from 5° to 45° with a scanning rate of 0.5° min^{-1}. In-plane and out-of-plane X-ray diffraction scans were measured by a Rigaku SmartLab X-ray diffractometer using Cu-K$_\alpha$ radiation (λ = 0.1542 nm) in the 2θ range from 5° to 35° with the scanning rate of 0.5° min^{-1}. The scanning electron micrographs of the morphologies of the nanosheets and membranes were measured by a JSM6700-F

instrument. Transmission electron microscope (TEM) images of the morphologies of nanosheets were measured by a Tecnai F20 instrument. An Asylum Research cypher atomic force microscope (AFM) was employed under ambient conditions in the high-amplitude mode (trapping mode). The Fourier transform infrared (FT-IR) spectra were recorded by a VERTEX 70 (Bruker) infrared spectrometer in the 400–4000 cm^{-1} frequency range, using KBr pellets. The nitrogen adsorption isotherms were measured at 77 K in the ASAP (Accelerated Surface Area and Porosimetry) 2020 System with the fragments of the membrane. The tensile property was tested using a Shimadzu Precision Universal Tester (AG-X plus 100 kN) with the constant speed of 50 μm min^{-1} using a load cell of 1 kN. The ~50-μm-thick membrane was cut to a ribbon with width of 0.5 cm and length of ~1.5 cm.

The structural model for Cu$_2$(CuTCPP) was constructed using the Materials Studio software package (Accelrys Inc.) by referring to Cu-TCPP [38,58]. The dimensions of the tetragonal unit cell, a = 1.65 nm, c = 0.91 nm, were determined from the selected area electron diffraction in TEM, and from the peaks of the in-plane and out-of-plane XRD patterns.

4.7. Electrochemical measurements

CR2032 coin cells were assembled in an Ar-filled glove box (< 1 ppm of O$_2$) by using the CB/S or CNT/S cathodes, modified Cu$_2$(CuTCPP)-Celgard separator, and Li foil anodes. The electrolyte was bis(trifluoromethanesulfonyl)imide lithium (1 M) in a mixed solvent of 1,2-dimethoxyethane and 1,3-dioxolane (v/v = 1:1) with LiNO$_3$ (2 wt%). The areal of the cathodes used in this work was about 1.13 cm^{-2}. To maintain consistency, the ratio of electrolyte to sulfur used for the CB/S and CNT/S cathodes was controlled to be 10 μL mg^{-1}. The ratio of electrolyte to sulfur used for the CB/S cathode can be reduced to 6 μL mg^{-1} without affecting the capacity (Fig. S20). Electrochemical measurements were performed using a LAND-CT2001C battery test system.

Conflict of interest

The authors declare no competing interests.

Appendix A. Supplementary material

Supplementary data associated with this article can be found in the online version at doi:10.1016/j.ensm.2018.12.016.

References

[1] A. Manthiram, Y.Z. Fu, S.H. Chung, C.X. Zu, Y.S. Su, Rechargeable lithium-sulfur batteries, Chem. Rev. 114 (2014) 11751.
[2] Y.X. Yin, S. Xin, Y.G. Guo, L.J. Wan, Lithium-sulfur batteries: electrochemistry, materials, and prospects, Angew. Chem. Int. Ed. 52 (2013) 13186.
[3] Q. Pang, X. Liang, C.Y. Kwok, L.F. Nazar, Advances in lithium-sulfur batteries based on multifunctional cathodes and electrolytes, Nat. Energy 1 (2016) 16132.
[4] Z.W. Seh, Y.M. Sun, Q.F. Zhang, Y. Cui, Designing high-energy lithium-sulfur

batteries, Chem. Soc. Rev. 45 (2016) 5605.

[5] G.M. Zhou, K. Liu, Y.C. Fan, M.Q. Yuan, B.F. Liu, W. Liu, F.F. Shi, Y.Y. Liu, W. Chen, J. Lopez, D. Zhuo, J. Zhao, Y. Tsao, X.Y. Huang, Q.F. Zhang, Y. Cui, An aqueous inorganic polymer binder for high performance lithium-sulfur batteries with flame-retardant properties, ACS Cent. Sci. 4 (2018) 260.

[6] X. Ji, K.T. Lee, L.F. Nazar, A highly ordered nanostructured carbon-sulphur cathode for lithium-sulphur batteries, Nat. Mater. 8 (2009) 500.

[7] F. Pei, T.H. An, J. Zang, X.J. Zhao, X.L. Fang, M.S. Zheng, Q.F. Dong, N.F. Zheng, From hollow carbon spheres to N-doped hollow porous carbon bowls: rational design of hollow carbon host for Li-S batteries, Adv. Energy Mater. 6 (2016) 1502539.

[8] Z.M. Zheng, H.C. Guo, F. Pei, X. Zhang, X.Y. Chen, X.L. Fang, T.H. Wang, N.F. Zheng, High sulfur loading in hierarchical porous carbon rods constructed by vertically oriented porous graphene-like nanosheets for Li-S batteries, Adv. Funct. Mater. 26 (2016) 8952.

[9] J. Liang, Z.H. Sun, F. Li, H.M. Cheng, Carbon materials for Li-S batteries: functional evolution and performance improvement, Energy Storage Mater. 2 (2016) 76.

[10] Z. Li, H.B. Wu, X.W. Lou, Rational designs and engineering of hollow micro-/ nanostructures as sulfur hosts for advanced lithium-sulfur batteries, Energ. Environ. Sci. 9 (2016) 3061.

[11] X. Liu, J.Q. Huang, Q. Zhang, L.Q. Mai, Nanostructured metal oxides and sulfides for lithium-sulfur batteries, Adv. Mater. 29 (2017) 1601759.

[12] G.M. Zhou, H.Z. Tian, Y. Jin, X.Y. Tao, B.F. Liu, R.F. Zhang, Z.W. Seh, D. Zhuo, Y.Y. Liu, J. Sun, J. Zhao, C.X. Zu, S.C. Wu, Q.F. Zhang, Y. Cui, Catalytic oxidation of Li₂S on the surface of metal sulfides for Li-S batteries, PNAS 114 (2017) 840.

[13] F. Pei, L.L. Lin, D.H. Ou, Z.M. Zheng, S.G. Mo, X.L. Fang, N.F. Zheng, Self-supporting sulfur cathodes enabled by two dimensional carbon yolk-shell nanosheets for high energy-density lithium-sulfur batteries, Nat. Commun. 8 (2017) 482.

[14] C. Ye, L. Zhang, C.X. Guo, D.D. Li, A. Vasileff, H.H. Wang, S.Z. Qiao, A 3D hybrid of chemically coupled nickel sulfide and hollow carbon spheres for high performance lithium-sulfur batteries, Adv. Funct. Mater. 27 (2017) 1702524.

[15] W.Z. Bao, L.M. Liu, C.Y. Wang, S. Choi, D. Wang, G.X. Wang, Facile synthesis of crumpled nitrogen-doped MXene nanosheets as a new sulfur host for lithium-sulfur batteries, Adv. Energy Mater. 8 (2018) 1702485.

[16] H.D. Yuan, W.K. Zhang, J.G. Wang, G.M. Zhou, Z.Z. Zhuang, J.M. Luo, H. Huang, Y.P. Gan, C. Liang, Y. Xia, J. Zhang, X.Y. Tao, Facilitation of sulfur evolution reaction by pyridinic nitrogen doped carbon nanoflakes for highly-stable lithium-sulfur batteries, Energy Storage Mater. 10 (2018) 1.

[17] G.M. Zhou, L. Li, C.Q. Ma, S.G. Wang, Y. Shi, N. Koratkar, W.C. Ren, F. Li, H.M. Cheng, A graphene foam electrode with high sulfur loading for flexible and high energy Li-S batteries, Nano Energy 11 (2015) 356.

[18] Y.S. Su, A. Manthiram, Lithium sulphur batteries with a microporous carbon paper as a bifunctional interlayer, Nat. Commun. 3 (2012) 1166.

[19] S.H. Chung, A. Manthiram, Carbonized eggshell film as a natural polysulfide reservoir for highly reversible Li-S batteries, Adv. Mater. 26 (2014) 1360.

[20] J. Balach, T. Jaumann, M. Klose, S. Oswald, J. Eckert, L. Giebeler, Functional mesoporous carbon-coated separator for long-life, high-energy lithiumsulfur batteries, Adv. Funct. Mater. 25 (2015) 5285.

[21] T. Yim, S.H. Han, N.H. Park, M.S. Park, J.H. Lee, J. Shin, J.W. Choi, Y. Jung, Y.N. Jo, J.S. Yu, K.J. Kim, Effective polysulfide rejection by dipole-aligned BaTiO₃ coated separator for lithium-sulfur batteries, Adv. Funct. Mater. 26 (2016) 7817.

[22] K. Adil, Y. Belmabkhout, R.S. Pillai, A. Cadiau, P.M. Bhatt, A.H. Assen, G. Maurin, M. Eddaoudi, Gas/vapour separation using ultra-microporous metal-organic frameworks: insights into the structure/separation relationship, Chem. Soc. Rev. 46 (2017) 3402.

[23] E.D. Bloch, W.L. Queen, R. Krishna, J.M. Zadrozny, C.M. Brown, J.R. Long, Hydrocarbon separations in a metal-organic framework with open iron (II) coordination sites, Science 335 (2012) 1606.

[24] J.R. Li, J. Sculley, H.C. Zhou, Metal-organic frameworks for separations, Chem. Rev. 112 (2012) 869.

[25] B. Chen, S. Xiang, G. Qian, Metal-organic frameworks with functional pores for recognition of small molecules, Acc. Chem. Res. 43 (2010) 1115.

[26] S. Bureekaew, S. Horike, M. Higuchi, M. Mizuno, T. Kawamura, D. Tanaka, N. Yanai, S. Kitagawa, One-dimensional imidazole aggregate in aluminium porous coordination polymers with high proton conductivity, Nat. Mater. 8 (2009) 831.

[27] L. Sun, M.G. Campbell, M. Dincă, Electrically conductive porous metal–organic frameworks, Angew. Chem. Int. Ed. 55 (2016) 3566.

[28] R. Demir-Cakan, M. Morcrette, F. Nouar, C. Davoisne, T. Devic, D. Gonbeau, R. Dominko, C. Serre, G. Ferey, J.M. Tarascon, Cathode composites for Li–S batteries via the use of oxygenated porous architectures, J. Am. Chem. Soc. 133 (2011) 16154.

[29] J. Zhou, R. Li, X. Fan, Y. Chen, R. Han, W. Li, J. Zheng, B. Wang, X. Li, Rational design of a metal-organic framework host for sulfur storage in fast, long-cycle Li-S batteries, Energy Environ. Sci. 7 (2014) 2715.

[30] J. Zheng, J. Tian, D. Wu, M. Gu, W. Xu, C. Wang, F. Gao, Lewis acid-base interactions between polysulfides and metal organic framework in lithium sulfur

batteries, Nano Lett. 14 (2014) 2345.

[31] H.Q. Jiang, X.C. Liu, Y.S. Wu, Y.F. Shu, X. Gong, F.S. Ke, H.X. Deng, Metal-organic frameworks for high charge-discharge rates in lithium-sulfur batteries, Angew. Chem. Int. Ed. 57 (2018) 3916.

[32] S. Bai, X. Liu, K. Zhu, S. Wu, H. Zhou, Metal-organic framework-based separator for lithium–sulfur batteries, Nat. Energy 1 (2016) 16094.

[33] S. Qiu, M. Xue, G. Zhu, Metal-organic framework membranes: from synthesis to separation application, Chem. Soc. Rev. 43 (2014) 6116.

[34] S. Sorribas, P. Gorgojo, C. Tellez, J. Coronas, A.G. Livingston, High flux thin film nanocomposite membranes based on metal–organic frameworks for organic solvent nanofiltration, J. Am. Chem. Soc. 135 (2013) 15201.

[35] G. Xu, K. Otsubo, T. Yamada, S. Sakaida, H. Kitagawa, Superprotonic conductivity in a highly oriented crystalline metal-organic framework nanofilm, J. Am. Chem. Soc. 135 (2013) 7438.

[36] D. Zacher, O. Shekhah, C. Woll, R.A. Fischer, Thin films of metal–organic frameworks, Chem. Soc. Rev. 38 (2009) 1418.

[37] F. Favier, E.C. Walter, M.P. Zach, T. Benter, R.M. Penner, Hydrogen sensors and switches from electrodeposited palladium mesowire arrays, Science 293 (2001) 2227.

[38] I. Hod, W. Bury, D.M. Karlin, P. Deria, C.W. Kung, M.J. Katz, M. So, B. Klahr, D. Jin, Y.W. Chung, T.W. Odom, O.K. Farha, J.T. Hupp, Directed growth of electroactive metal-organic framework thin films using electrophoretic deposition, Adv. Mater. 26 (2014) 6295.

[39] K.S. Novoselov, V.I. Fal'ko, L. Colombo, P.R. Gellert, M.G. Schwab, K. Kim, A roadmap for graphene, Nature 490 (2012) 192.

[40] X. Peng, L. Peng, C. Wu, Y. Xie, Two dimensional nanomaterials for flexible supercapacitors, Chem. Soc. Rev. 43 (2014) 3303.

[41] Z. Sun, T. Liao, Y. Dou, S.M. Hwang, M.S. Park, L. Jiang, J.H. Kim, S.X. Dou, Generalized self-assembly of scalable two-dimensional transition metal oxide nanosheets, Nat. Commun. 5 (2014) 3813.

[42] C.L. Tan, X.H. Cao, X.J. Wu, Q.Y. He, J. Yang, X. Zhang, J. Chen, W. Zhao, S.K. Han, G.H. Nam, M. Sindoro, H. Zhang, Recent advances in ultrathin two-dimensional nanomaterials, Chem. Rev. 117 (2017) 6225.

[43] J.J. Richardson, M. Björnmalm, F. Caruso, Technology-driven layer-by-layer assembly of nanofilms, Science 348 (2015) aaa2491.

[44] F. Liu, T.S. Seo, A controllable self-assembly method for large-scale synthesis of graphene sponges and free-standing graphene films, Adv. Funct. Mater. 20 (2010) 1930.

[45] S. Korkut, J.D. Roy-Mayhew, D.M. Dabbs, D.L. Milius, I.A. Aksay, High surface area tapes produced with functionalized graphene, ACS Nano 5 (2011) 5214.

[46] T. Rodenas, I. Luz, G. Prieto, B. Seoane, H. Miro, A. Corma, F. Kapteijn, F.X. Llabres, i Xamena, J. Gascon, Metal-organic framework nanosheets in polymer composite materials for gas separation, Nat. Mater. 14 (2015) 48.

[47] M. Hu, S. Ishihara, Y. Yamauchi, Bottom-up synthesis of monodispersed single-crystalline cyano-bridged coordination polymer nanoflakes, Angew. Chem. Int. Ed. 52 (2013) 1235.

[48] P.Z. Li, Y. Maeda, Q. Xu, Top-down fabrication of crystalline metal-organic framework nanosheets, Chem. Commun. 47 (2011) 8436.

[49] Y. Peng, Y. Li, Y. Ban, H. Jin, W. Jiao, X. Liu, W. Yang, Metal-organic framework nanosheets as building blocks for molecular sieving membranes, Science 346 (2014) 1356.

[50] R. Dong, M. Pfeffermann, H. Liang, Z. Zheng, X. Zhu, J. Zhang, X. Feng, Large-area, free-standing, two-dimensional supramolecular polymer single-layer sheets for highly efficient electrocatalytic hydrogen evolution, Angew. Chem. Int. Ed. 54 (2015) 12058.

[51] M. Zhao, Y. Wang, Q. Ma, Y. Huang, X. Zhang, J. Ping, Z. Zhang, Q. Lu, Y. Yu, H. Xu, Y. Zhao, H. Zhang, Ultrathin 2D metal-organic framework nanosheets, Adv. Mater. 27 (2015) 7372.

[52] L. Cao, Z. Lin, F. Peng, W. Wang, R. Huang, C. Wang, J. Yan, J. Liang, Z. Zhang, T. Zhang, L. Long, J. Sun, W. Lin, Self-supporting metal–organic layers as single-site solid catalysts, Angew. Chem. Int. Ed. 55 (2016) 4962.

[53] G.M. Zhou, S.F. Pei, L. Li, D.W. Wang, S.G. Wang, K. Huang, L.C. Yin, F. Li, H.M. Cheng, A graphene-pure-sulfur sandwich structure for ultrafast, long-life lithium-sulfur batteries, Adv. Mater. 26 (2014) 625.

[54] J. Sun, Y. Sun, M. Pasta, G. Zhou, Y. Li, W. Liu, F. Xiong, Y. Cui, Entrapment of polysulfides by a black-phosphorus-modified separator for lithium-sulfur batteries, Adv. Mater. 28 (2016) 9797.

[55] Z.A. Ghazi, X. He, A.M. Khattak, N.A. Khan, B. Liang, A. Iqbal, J. Wang, H. Sin, L. Li, Z. Tang, MoS₂/Celgard separator as efficient polysulfide barrier for long-life lithiumsulfur batteries, Adv. Mater. 29 (2017) 1606817.

[56] F. Pei, L.L. Lin, A. Fu, S.G. Mo, D.H. Ou, X.L. Fang, N.F. Zheng, A Two-dimensional porous carbon-modified separator for high-energy-density Li-S batteries, Joule 2 (2018) 323.

[57] R. Fang, S. Zhao, Z. Sun, W. Wang, H.M. Cheng, F. Li, More reliable lithium-sulfur batteries: status, solutions and prospects, Adv. Mater. 29 (2017) 1606823.

[58] G. Xu, T. Yamada, K. Otsubo, S. Sakaida, H. Kitagawa, Facile "modular assembly" for fast construction of a highly oriented crystalline MOF nanofilm, J. Am. Chem. Soc. 134 (2012) 16524.